Surface & Coatings Technology 424 (2021) 127657

Contents lists available at ScienceDirect

Surface & Coatings Technology

journal homepage: www.elsevier.com/locate/surfcoat

Laser nitriding of Zr-based metallic glass: An investigation by orthogonal experiments

Jing Hong [a], Yongfeng Qian [a], Lin Zhang [b], Hu Huang [a,*], Minqiang Jiang [c,d], Jiwang Yan [b]

[a] Key Laboratory of CNC Equipment Reliability, Ministry of Education, School of Mechanical and Aerospace Engineering, Electron Microscopy Center, Jilin University, Changchun, Jilin 130022, China
[b] Department of Mechanical Engineering, Faculty of Science and Technology, Keio University, Yokohama 223-8522, Japan
[c] State Key Laboratory of Nonlinear Mechanics, Institute of Mechanics, Chinese Academy of Sciences, Beijing 100190, China
[d] School of Engineering Science, University of Chinese Academy of Sciences, Beijing 100049, China

ARTICLE INFO

Keywords:
Laser nitriding
Metallic glass
Orthogonal experiment
Surface hardness

ABSTRACT

Laser nitriding is a useful method to improve the surface hardness of materials, and it has been newly introduced to harden the surface of Zr-based metallic glass (MG). However, the currently achieved improvement in surface hardness is only 15.7%. To explore the potential of laser nitriding of Zr-based MG, orthogonal experiments were designed and performed in this study. By nanosecond pulsed laser irradiation in nitrogen atmosphere, the effects of laser parameters (average laser power, scanning speed, overlap rate and number of irradiation cycle) on the surface hardness of Zr-based MG were systematically investigated. The experimental results showed the highest surface hardness reached 18.21 GPa (Meyer's hardness) by orthogonal design, which is about 2 times higher than that of the as-cast MG. Furthermore, the laser affecting layer consisting of nitride phase reached tens of microns. The obtained results demonstrated that significant improvement in surface hardness could be achieved by selecting appropriate laser irradiation parameters, which would be beneficial to the engineering applications of MGs as surface contact materials.

1. Introduction

Due to the long-range disordered and short-range ordered atomic structure, metallic glasses (MGs) present superior mechanical, physical and chemical properties, such as high strength, hardness, and excellent corrosion resistance [1–4]. Therefore, MGs are very promising materials for application in aerospace, precision machinery, electronic frames and so on [5–7]. However, the limited tensile plasticity of MGs still greatly hinders their applications as structural and engineering materials [8–10]. On the other hand, the relatively high hardness of MGs compared to many crystalline alloys, opens a new window for their applications as surface functional materials. For this kind of application, further improving their hardness is meaningful.

Laser nitriding is commonly recognized as an effective method to improve the hardness of materials [11–15], and it has been newly applied to harden the surface of Zr-based MG [16]. As reported in Ref. [16], when irradiated in nitrogen atmosphere by nanosecond pulsed laser with appropriate experiment parameters, laser nitriding of Zr-based MG occurred, resulting in the surface hardening. However, as the laser irradiation parameters were not optimized, the maximum improvement in surface hardness was only 15.7% [16]. So, the question is whether a higher surface hardness can be obtained by optimizing the laser irradiation parameters.

To answer this question, by orthogonal design [17–19], systematic laser nitriding experiments were performed in nitrogen atmosphere to investigate the effects of laser parameters (i.e., average laser power, scanning speed, overlap rate, and number of irradiation cycle) on the surface hardness of Zr-based MG. The orthogonal experimental results indicated that under some given laser parameters, the surface hardness of laser nitrided Zr-based MG was almost three times of the hardness of the as-cast MG surface (i.e. the hardness was nearly increased by 200%). Furthermore, the effects of laser nitriding on the surface shear bands and serrated flows of Zr-based MG during nanoindentation testing were studied, and the hardening mechanism was discussed as well.

* Corresponding author.
E-mail address: huanghu@jlu.edu.cn (H. Huang).

https://doi.org/10.1016/j.surfcoat.2021.127657
Received 20 June 2021; Received in revised form 7 August 2021; Accepted 24 August 2021
Available online 27 August 2021

2. Materials and experiments

2.1. Material and experimental procedures

The Zr-based MG plate ($Zr_{41.2}Ti_{13.8}Cu_{12.5}Ni_{10}Be_{22.5}$) with the size of 20 mm × 20 mm × 2 mm was used in the study. This sample was bought from Peshing New Metal Material (Changzhou) Co., Ltd., China. To remove the surface oxide layer and obtain flat surface, the sample was mechanically ground with 400, 800, 1200, and 2000 grit sand papers in sequence by the precision lapping/polishing machine (UNIPOL-802, MTI corporation, China), then polished with diamond abrasive paste, and finally cleaned by acetone and alcohol.

A fiber nanosecond pulsed laser system (SP-050P-A-EP-Z-F-Y, SPI Lasers, UK Ltd.) (laser wavelength: 1064 nm, pulse width: 10 ns, repetition frequency: 600 kHZ, laser beam diameter: ~43 μm) was employed to irradiate the MG surface. The sample was placed in a reaction chamber with nitrogen atmosphere. To ensure comparability of the hardness of laser-irradiated surfaces, all the experiments designed by orthogonal array were performed on the same sample.

After laser irradiation, the topographies of laser-irradiated surfaces were observed by using the tungsten filament scanning electron microscope (SEM, JSM-IT500A, JEOL, Japan). The surface hardness of the as-cast MG and laser-irradiated surfaces were characterized by the nanoindentation instrument (DUH-211, SHIMADZU, Japan) equipped with the standard data processing software based on the Oliver-Pharr (OP) method [20]. During nanoindentation testing, a pyramidal indenter with an angle of 115° between the ridge and face (pyramidal indenter, TOKYO DIAMOND Tools MFG. Co., Ltd., Japan) was employed, and the indentation load and the loading rate were 120 mN and 10 mN/s, respectively. After the nanoindentation tests, the indentation morphologies were captured via SEM. The element contents of the as-cast MG and laser-irradiated surfaces were characterized by an energy dispersive X-ray spectroscopy (EDS, EX-74600U4L2Q, JEOL, Japan), and the employed acceleration voltage, working distance (WD), and real time were 15.0 kV, 9.9 mm and 63.05 s, respectively. The phase compositions were characterized by an X-ray diffractometer (XRD, D8 Discover, Bruker, Germany). The 2θ angle was scanned from 10° to 80° with a scanning speed of 25°/min.

2.2. Design of orthogonal experiments

For designing the orthogonal experiments, the first step is to determine the laser parameters (i.e., average laser power, scanning speed, overlap rate and number of irradiation cycle) and the corresponding levels. In order to fully evaluate the influence of laser parameters on surface hardness of Zr-based MG, the average laser power, scanning speed, and overlap rate were selected as eight-level. However, when the MG surface was repeatedly irradiated over four cycles, extremely severe ablation occurred, so the number of irradiation cycle was set to be four-level. To ensure the accuracy of results, the interval values between two adjacent levels basically remained the same for these four parameters, as shown in Table 1. Accordingly, a $L_{64}(4 \times 8^3)$ orthogonal array was obtained to guide the subsequent experiments as listed in Table 2. During the orthogonal experiments, the notations (A, B, C, and D) represent the average laser power, scanning speed, overlap rate, and number of irradiation cycle, respectively.

3. Results and discussion

3.1. Hardness obtained by orthogonal experiments

After laser irradiation in nitrogen atmosphere under the above experimental conditions, the surface quality of the ablated MG surface was deteriorated. Therefore, the irradiated surfaces were polished to obtain smooth regions, where nanoindentation tests were performed. The nanoindentation hardness was obtained by fitting and analyzing the load-depth curves according to the OP method. To ensure the accuracy of experimental results, five nanoindentation tests were performed for each experimental condition. The hardness and corresponding standard deviation are listed in Table 3. For the as-cast MG surface, the average hardness is 6.50 GPa with small standard deviation, which proves that the mechanical properties of the as-cast MG are relatively uniform. While, for the laser-irradiated surfaces, the average hardness values are quite different, ranging from 5.60 GPa to 24.68 GPa. For No. 9, the surface hardness is less than that of the as-cast MG surface, which may be due to the softening effect caused by the laser thermal shock [16,21]. For No. 18, the surface hardness significantly increases to 11.62 GPa. Especially, for No. 34, the surface hardness reaches the maximum of 24.68 GPa, increasing by approximately three times compared to the as-cast MG.

3.2. Effects of laser parameters on surface hardness

According to the results listed in Table 3, the hardness of laser-irradiated surfaces strongly depends on the laser parameters. Therefore, the effects of laser parameters on surface hardness are further analyzed. To facilitate the analysis, the involved symbols and expressions are defined firstly.

K_{mij} is defined as a test index (hardness) corresponding to the ith laser parameter at level m, j stands for the jth experiment, and K_{mi} is taken as the sum of test indexes at level m for the ith laser parameter. Its formula is defined as $\sum_j^N K_{mij} = K_{mi}$, where N is the total number of experiments at level m for the ith laser parameter.

k_{mi} (average hardness) stands for the mean of K_{mi}, and its formula is defined as $k_{mi} = K_{mi}/N$. Accordingly, the average hardness for these four laser parameters at different levels are shown in Table 4.

Fig. 1 presents average hardness (k_{mi}) changing with the laser parameters. As illustrated in Fig. 1(a), the average hardness is significantly increased from 6.06 GPa to 12.78 GPa when increasing the average laser power. While, as the scanning speed increases from 10 mm/s to 30 mm/s, the average hardness drops sharply from 14.31 GPa to 9.29 GPa, and then fluctuates up and down until 80 mm/s, as observed in Fig. 1(b). In Fig. 1(c), the variation trend of surface hardness is not visible, but the overlap rate of 70% is slightly superior to other levels. Being similar to Fig. 1(a), the average hardness in Fig. 1(d) gradually increases when the number of irradiation cycles is increased from 1 to 4. In view of the variation degree of average hardness, it can be concluded that the average laser power and scanning speed have a stronger influence on surface hardness compared to the overlap rate and number of irradiation cycle. Furthermore, it is noted that when the average laser power, scanning speed, overlap rate, and number of irradiation cycle are 12.1 W (A_8), 10 mm/s (B_1), 70% (C_7), and 4 (D_4), respectively, the surface hardness achieves the maximum for each laser parameter.

Table 1
Laser parameters with different levels.

Parameters	Notations	Levels							
		1	2	3	4	5	6	7	8
Average laser power (W)	A	0.8	2.2	3.8	5.4	7.1	8.8	10.5	12.1
Scanning speed (mm/s)	B	10	20	30	40	50	60	70	80
Overlap rate (%)	C	10	20	30	40	50	60	70	80
Number of irradiation cycle	D	1	2	3	4				

Table 2
Design of orthogonal experiments.

Run. no	Laser parameters and levels			
	A	B	C	D
1	1 (0.8)	8 (80)	1 (10)	1 (1)
2	1	1 (10)	4 (40)	3 (3)
3	1	2 (20)	7 (70)	1 (1)
4	1	3 (30)	6 (60)	3 (3)
5	1	4 (40)	2 (20)	2 (2)
6	1	5 (50)	3 (30)	4 (4)
7	1	6 (60)	8 (80)	2 (2)
8	1	7 (70)	5 (50)	4 (4)
9	2 (2.2)	8	3	4
10	2	1	2	2
11	2	2	5	4
12	2	3	8	2
13	2	4	4	3
14	2	5	1	1
15	2	6	6	3
16	2	7	7	1
17	3 (3.8)	8	5	3
18	3	1	8	1
19	3	2	3	3
20	3	3	2	1
21	3	4	6	4
22	3	5	7	2
23	3	6	4	4
24	3	7	1	2
25	4 (5.4)	8	7	2
26	4	1	6	4
27	4	2	1	2
28	4	3	4	4
29	4	4	8	1
30	4	5	5	3
31	4	6	2	1
32	4	7	3	3
33	5 (7.1)	8	6	2
34	5	1	7	4
35	5	2	4	2
36	5	3	1	4
37	5	4	5	1
38	5	5	8	3
39	5	6	3	1
40	5	7	2	3
41	6 (8.8)	8	8	3
42	6	1	5	1
43	6	2	2	3
44	6	3	3	1
45	6	4	7	4
46	6	5	6	2
47	6	6	1	4
48	6	7	4	2
49	7 (10.5)	8	2	4
50	7	1	3	2
51	7	2	8	4
52	7	3	5	2
53	7	4	1	3
54	7	5	4	1
55	7	6	7	3
56	7	7	6	1
57	8 (12.1)	8	4	1
58	8	1	1	3
59	8	2	6	1
60	8	3	7	3
61	8	4	3	2
62	8	5	2	4
63	8	6	5	2
64	8	7	8	4

In order to explore whether surface hardness could be further improved, a combination ($A_8B_1C_7D_4$) was experimentally investigated. The results showed that extremely severe ablation occurred on the Zr-based MG surface (not shown here), resulting in collapse of surface material. This phenomenon may be caused by the interaction of different parameters on surface hardness. To confirm the state, the interaction between any two laser parameters is analyzed, and the

Table 3
The hardness results corresponding to the orthogonal experiments.

Run. no	Average hardness (GPa)	Standard deviation	Run. no	Average hardness (GPa)	Standard deviation
1	6.21	0.112	33	8.41	0.528
2	6.10	0.101	34	24.68	3.849
3	6.25	0.078	35	9.96	1.816
4	6.32	0.095	36	9.49	0.745
5	6.15	0.103	37	8.34	0.372
6	6.34	0.688	38	9.69	1.203
7	6.22	0.095	39	7.84	0.226
8	6.38	0.096	40	8.65	0.036
9	5.83	0.068	41	9.23	0.188
10	5.60	0.123	42	12.61	1.734
11	6.56	0.577	43	12.60	1.690
12	6.00	0.079	44	8.14	0.406
13	6.34	0.502	45	11.34	1.631
14	6.00	0.078	46	11.54	2.012
15	6.13	0.618	47	9.08	0.351
16	6.03	0.247	48	8.40	0.653
17	6.70	0.592	49	8.79	0.490
18	11.62	1.649	50	19.72	2.094
19	10.36	0.855	51	17.15	2.051
20	6.67	0.755	52	12.37	1.929
21	8.32	0.604	53	12.63	1.498
22	7.42	0.788	54	9.94	1.120
23	6.84	0.307	55	10.95	1.088
24	6.00	0.534	56	9.37	0.534
25	8.87	0.909	57	9.49	0.609
26	18.67	2.114	58	15.43	2.264
27	10.46	0.998	59	14.33	1.253
28	10.53	0.800	60	14.82	2.785
29	8.41	0.251	61	11.66	1.192
30	8.75	0.533	62	12.12	0.637
31	7.34	0.055	63	9.92	0.719
32	9.53	0.265	64	14.44	1.033
As-cast MG	6.50	0.07			

Table 4
Average hardness corresponding to these four laser parameters with different levels.

Average hardness	Laser parameters			
	A	B	C	D
k_{1i}	As-cast	14.31	9.42	7.67
k_{2i}	6.06	10.95	8.49	8.23
k_{3i}	7.99	9.29	9.93	8.53
k_{4i}	10.32	9.15	8.45	9.76
k_{5i}	10.88	8.97	8.96	
k_{6i}	10.49	8.04	9.62	
k_{7i}	12.62	9.35	11.29	
k_{8i}	12.78	7.95	10.35	

interaction diagram is illustrated in Fig. 2. As reported in Ref. [22], if the curves in the interaction diagram cross, the corresponding parameters interact with each other. It can be concluded that the selected laser parameters have an interactive effect on surface hardness. Nevertheless, the surface hardness obtained by orthogonal experiments has been significantly improved compared to the previous studies [23,24].

3.3. Morphologies of laser-irradiated surfaces after mechanical polishing

Apart from the change in hardness of laser-irradiated surfaces, the corresponding surface morphologies would be also different. With consideration of numerous experiments, eight representative groups (Nos. 8, 11, 18, 26, 34, 42, 50, and 58) with the highest hardness for each laser power in Table 2 are selected for comparative analysis. However, after mechanically polishing the processed sample, the affecting layers obtained at the laser power of 0.8 W have been completely removed, as

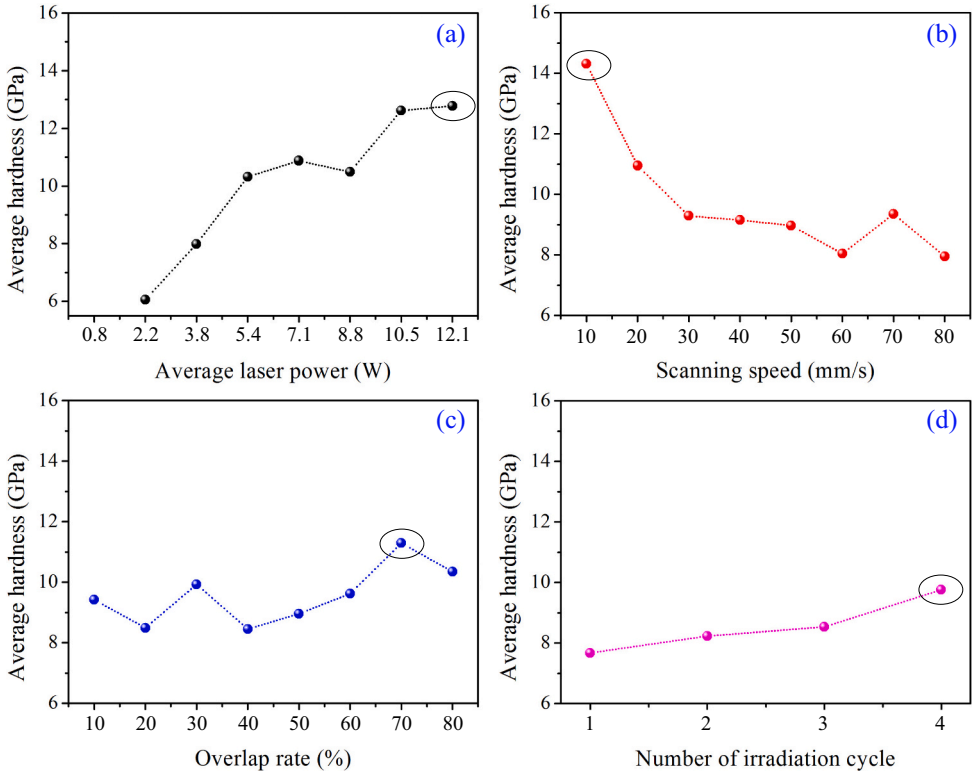

Fig. 1. Effects of (a) average laser power, (b) scanning speed, (c) overlap rate, and (d) number of irradiation cycle on the average hardness.

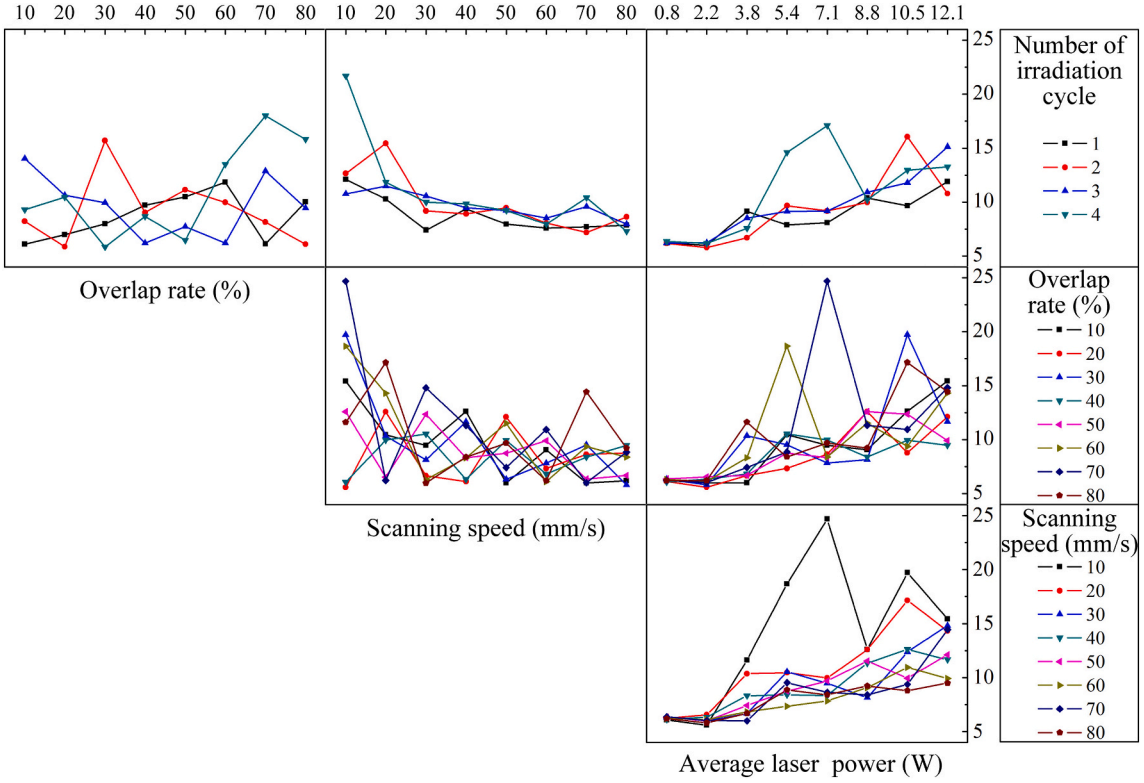

Fig. 2. Interaction diagram between different laser parameters.

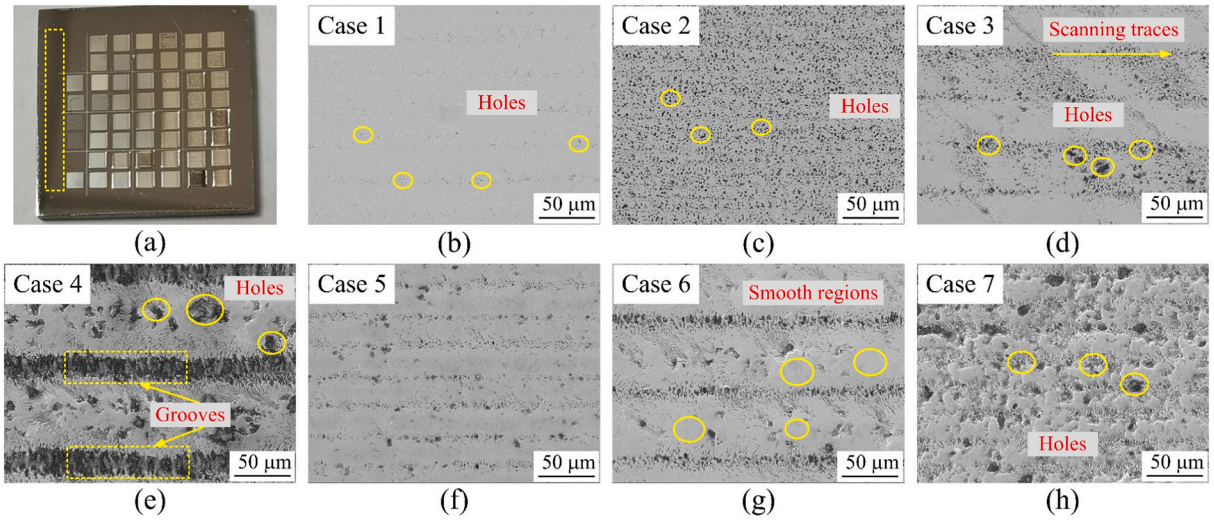

Fig. 3. (a) Optical morphology of all the laser-irradiated surfaces obtained by orthogonal experiments. (b)–(h) SEM morphologies of the laser-irradiated surfaces corresponding to experimental conditions in Table 5: (b) case 1, (c) case 2, (d) case 3, (e) case 4, (f) case 5, (g) case 6, and (h) case 7.

Table 5
Laser parameters corresponding to the selected cases.

Case	A	B	C	D	Average hardness (GPa)
Case 1	2.2	20	50	4	6.56
Case 2	3.8	10	80	1	11.62
Case 3	8.8	10	50	1	12.61
Case 4	12.1	10	10	3	15.43
Case 5	5.4	10	60	4	18.67
Case 6	10.5	10	30	2	19.72
Case 7	7.1	10	70	4	24.68

shown in Fig. 3(a). Therefore, this group (No. 8) is absent for comparative research, and the remained test groups are defined as cases 1 to 7, in the order of the increase in surface hardness, as shown in Table 5.

As shown in Fig. 3, the SEM morphologies of the laser-irradiated surfaces (cases 1–7) after mechanical polishing are covered by holes, grooves, as well as the smooth regions where nanoindentation tests are performed. From case 1 to case 4, as the laser power gradually increases, the holes and the scanning traces become clear gradually, reflecting the ablation degree at different laser powers.

3.4. Morphologies of indentations

Fig. 4 shows the SEM morphologies of the indentations obtained on the as-cast MG and laser-irradiated surfaces (cases 1–7), and these SEM images have the same scale bar. It is clearly seen that the size of the indentation gradually decreases from case 1 to case 7, which directly proves that the surface hardness tends to increase from case 1 to case 7. Nevertheless, all the indentations for laser-irradiated surfaces are smaller than that for the as-cast MG, indicating the increase in surface hardness after laser irradiation in nitrogen atmosphere.

Although the OP method is the most commonly used method for calculating the nanoindentation hardness, this method is originally proposed for the indentation with sink-in behavior and then expanded to the indentation with pile-up. However, due to the pile-up behavior, the hardness is usually overestimated by the OP method [25]. In order to more accurately evaluate the hardness, the surface hardness (H) was also calculated by the formula $H = F/A$ according to the Meyer's hardness law, where F is the indentation load and A stands for the projected area of indentation morphology [26]. The indentation load is 120 mN and by measuring the projected contact lengths of indentation morphologies in Fig. 4, the projected areas for the as-cast MG and cases 1–7

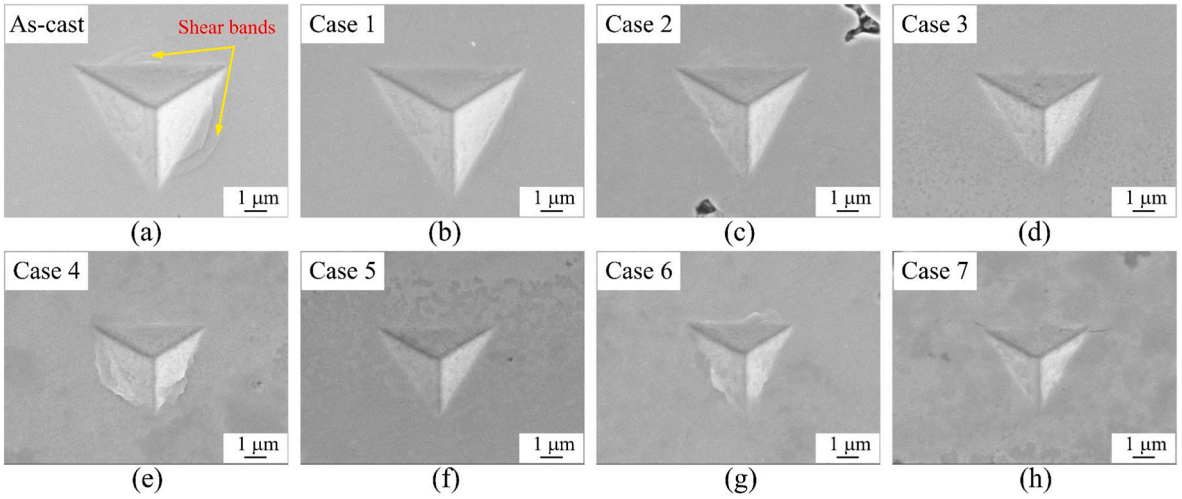

Fig. 4. Indentation morphologies of the as-cast MG and laser-irradiated surfaces (cases 1–7). The indentation load and loading rate are 120 mN and 2 mN/s, respectively.

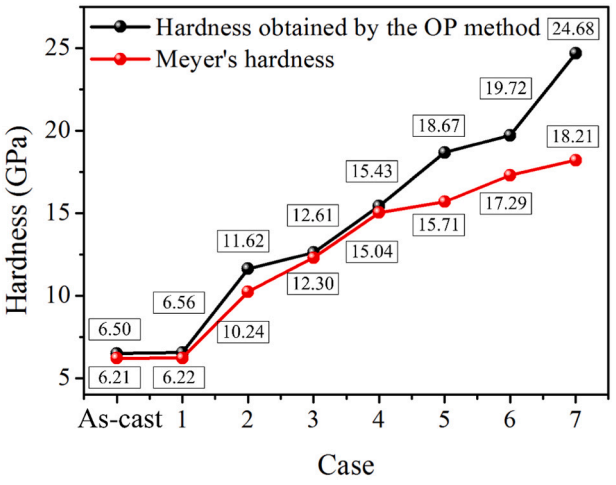

Fig. 5. Comparison between the Meyer's hardness and the hardness obtained by the OP method for the as-cast MG and cases 1–7.

are determined to be 19.32, 19.29, 11.72, 9.76, 7.98, 7.64, 6.94, and 6.59 μm^2, respectively. According to the above formula, Meyer's hardness is obtained as shown in Fig. 5. For comparison, the nanoindentation hardness calculated by the OP method is also depicted in Fig. 5. It is noted that for cases 1–4, the differences in hardness obtained by these two methods are minor; while, for cases 5, 6, and 7, the Meyer's hardness are obviously lower than nanoindentation hardness. This is due to the small indentation depth corresponding to the high hardness, and the measuring errors coming from the calibration of contact area as well as the pile-up would be remarkable. Fig. 6(a), (b) and (c) show the cross-sectional curves of indentations obtained for case 6, case 7 and as-cast MG, respectively. As illustrated in Fig. 6, the pile-ups are clearly observed for the as-cast MG, case 6, and case 7, which may lead to the difference between the Meyer's hardness and the hardness obtained by the OP method. Nevertheless, the variation trend of the hardness obtained by these two methods is consistent with each other, which further proves a significant increase in surface hardness after laser irradiation in nitrogen atmosphere.

3.5. EDS and XRD analysis

From the above analysis, it can be found that laser irradiation in nitrogen atmosphere could result in significant increase in surface hardness. It has been reported that laser irradiation without nitrogen atmosphere could cause thermal shock and the increase in free volume, resulting in surface softening [27,28]; while the increase in surface hardness is related to the introduction of ZrN phase [16,29]. Thus, it is conjectured that more ZrN phase has been produced on the irradiated surface with higher hardness. To confirm this, the EDS point tests were carried out to measure the element contents of the laser-irradiated surfaces after mechanical polishing. To ensure the reliable results, three EDS point tests were performed for each laser-irradiated surface. For comparison, the element contents of the as-cast MG surface were also measured. Be, as a light element, cannot be detected. Taking the as-cast MG, case 6, and case 7 for examples, the average atomic percent of each element is listed in Table 6. It is seen that N element is not detected for the as-cast MG, but it appears for case 6 and case 7. Furthermore, the N element content for case 7 is higher than that for case 6. To further confirm the phase generated during laser irradiation in nitrogen atmosphere, the above cases were also characterized by XRD. As shown in Fig. 7, the typical amorphous characteristics are exhibited for the as-cast MG; while the peaks of ZrN phase are clearly observed in the patterns of case 6 and case 7. Being similar to the variation of N element content, the peak intensity of ZrN phase tends to gradually increase from case 6 to case 7. Apart from the ZrN peaks, some TiN peaks are also observed in Fig. 7; however, compared to the ZrN peaks, the TiN peaks are very weak, so its effect on the surface hardness would be quite slight. Taking these analyses and the aforementioned results of surface hardness into consideration, it can be concluded that the increase in surface hardness is mainly caused by the ZrN phase during laser irradiation in nitrogen atmosphere, which further depends on the laser irradiation parameters.

Table 6
Element contents for the as-cast MG and laser-irradiated surfaces (case 6 and case 7) after mechanical polishing.

Element	Zr (at.%)	Ti (at.%)	Cu (at.%)	Ni (at.%)	N (at.%)
As-cast MG	55.06	22.38	12.89	9.67	0
Case 6	38.99	27.90	11.89	11.51	9.71
Case 7	43.27	25.94	5.99	5.09	19.71

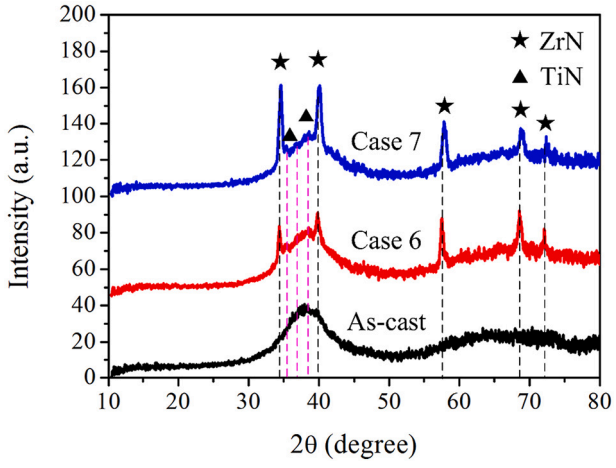

Fig. 7. XRD patterns obtained for the as-cast MG and laser-irradiated surfaces (case 6 and case 7) after mechanical polishing.

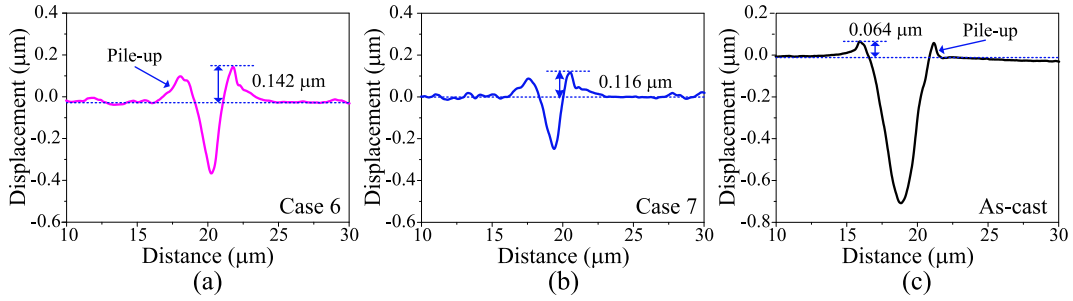

Fig. 6. Cross-sectional curves of indentation morphologies corresponding to (a) case 6, (b) case 7, and (c) as-cast MG.

3.6. Shear bands and serrated flow

Apart from the change in surface hardness, the obvious change in surface shear bands has been found after laser irradiation in nitrogen atmosphere. As shown in Fig. 4, remarkable shear bands appear around the indentation obtained on the as-cast MG surface, but they almost disappear for all the laser-irradiated surfaces. According to the previous studies [30–32], the variation in surface shear bands generally indicates that micro-scale plastic deformation of MG has been changed. To further evaluate the influence of laser irradiation on the micro-scale plastic deformation of MG, the load-depth curve and serrated flow will be further analyzed [33,34].

The load-depth curves of the as-cast MG and laser-irradiated surfaces (cases 1–7) obtained under the indentation load of 120 mN and loading rate of 2 mN/s are illustrated in Fig. 8. To clearly characterize the serrated flow, the enlarged images of the load-depth curves in the load range of 90 to 120 mN corresponding to the as-cast MG and cases 1–7 are shown in Fig. 8(b), (d), (f), (h), (j), (l), (n), and (p), respectively. It is observed that serrated flows are clearly presented in the loading curve for the as-cast MG surface. However, for cases 1–7, the serrated flows are significantly weakened. Especially, from case 2 to case 7, almost no serrated flows are observed.

To further quantitatively analyze the number and intensity of the serrated flows, the depth difference-load curve is employed [16], and the

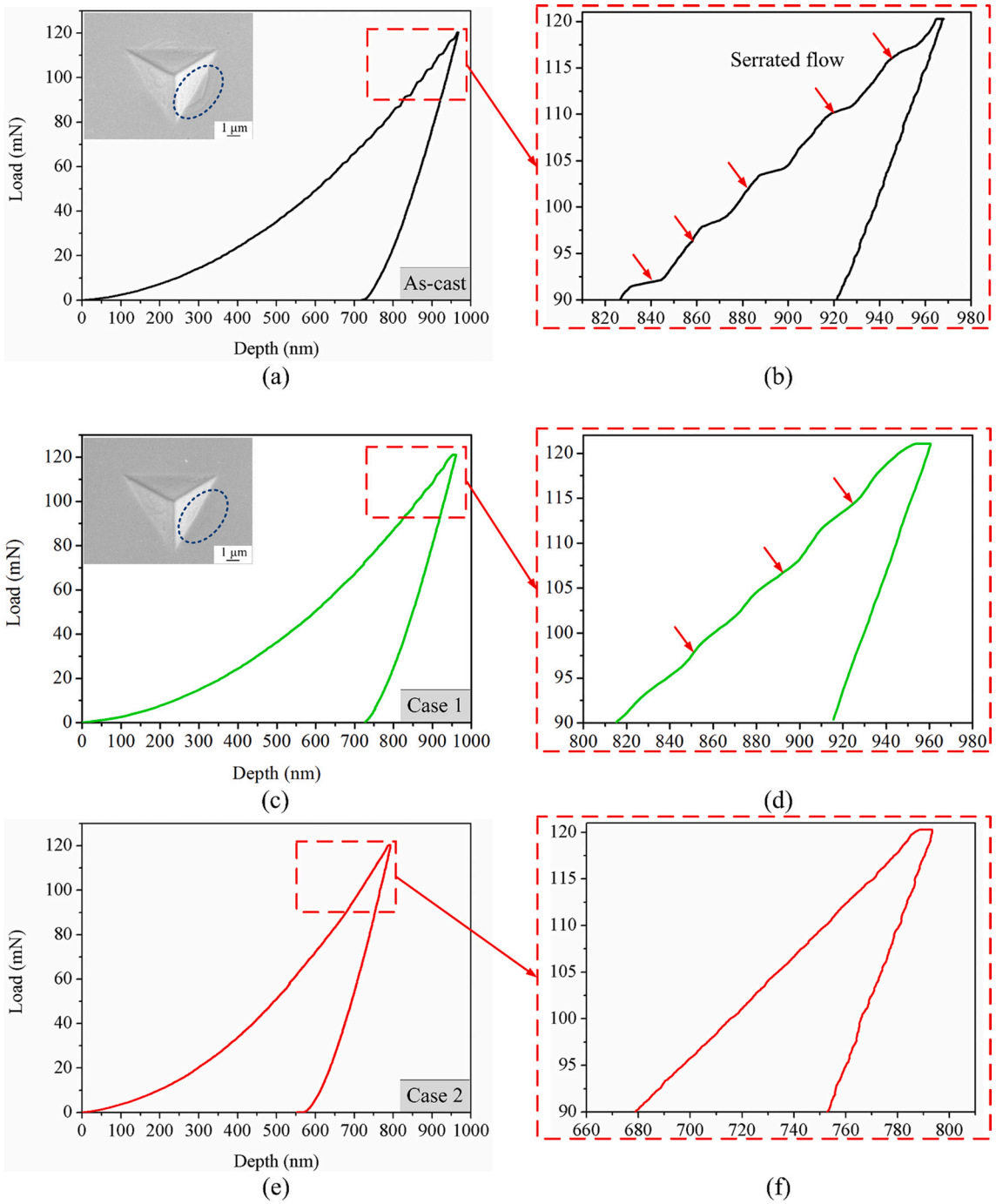

Fig. 8. Load-depth curves of the as-cast MG and laser-irradiated surfaces obtained under the indentation load of 120 mN: (a–b) as-cast, (c–d) case 1, (e–f) case 2, (g–h) case 3, (i–j) case 4, (k–l) case 5, (m–n) case 6, and (o–p) case 7.

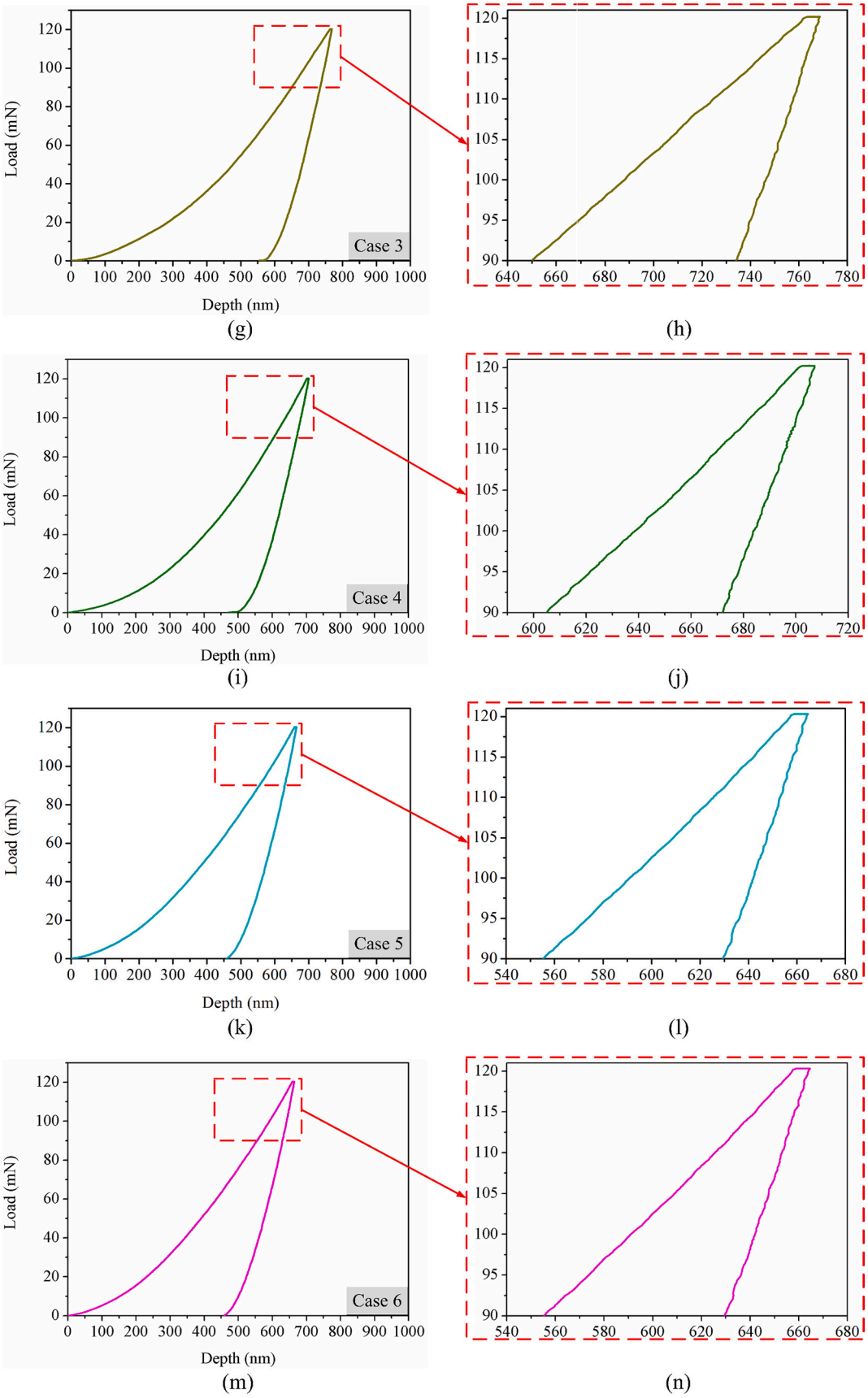

Fig. 8. (*continued*).

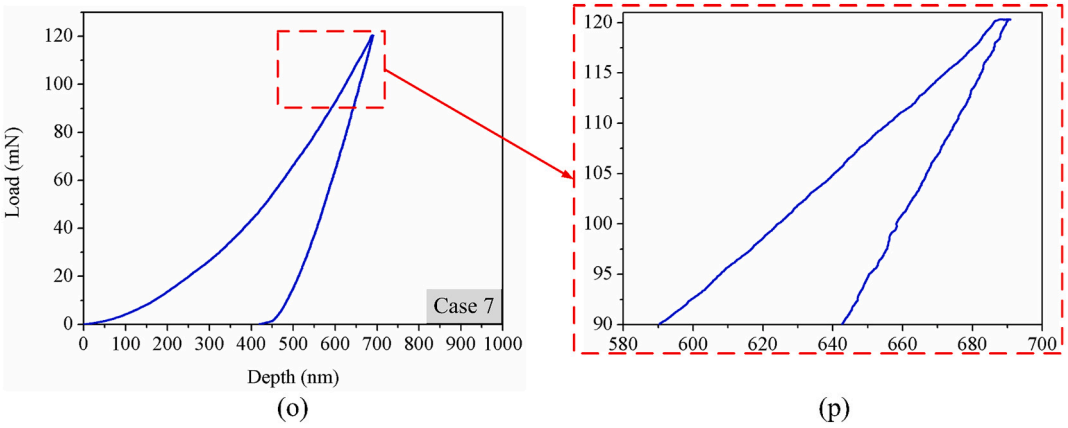

Fig. 8. (*continued*).

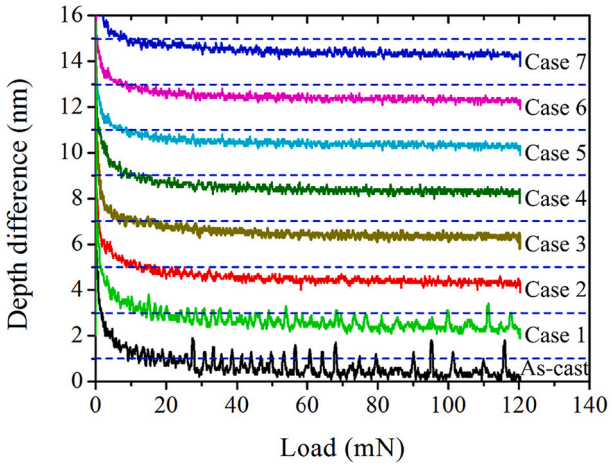

Fig. 9. Depth difference-load curves of the as-cast MG and laser-irradiated surfaces.

corresponding curves are presented in Fig. 9. A serrated flow in the load-depth curve corresponds to a peak of the depth difference-load curve, and the intensity of the peak is affected by the size of serrated flow. As illustrated in Fig. 9, for the as-cast MG surface, the number of peaks with a depth difference being over 1 nm in the load range of 20 to 120 mN is 25. However, for case 1, the number of peaks is sharply reduced to 13, and for cases 2-7, no obvious peaks are observed. The above results demonstrate that the serrated flows and the surface shear bands have been significantly suppressed after laser irradiation in nitrogen atmosphere, i.e. the micro-scale plastic deformation of MG has been changed. According to some previous studies [35,36], this change in micro-scale plastic deformation should be attributed to the coupling effects of laser thermal shock and the introduction of secondary phase (ZrN).

3.7. Cross-sectional analysis

The above results suggest that an affecting layer consisting of nitride phases could have been formed on the MG surface after laser irradiation in nitrogen atmosphere. For practical surface engineering applications, the thickness of the affecting layer determines its service time. Therefore, taking the case 6 and case 7 for examples, the cross-sectional analysis of the laser-irradiated regions before and after mechanical polishing is performed. These cross-sections were obtained by low-speed diamond cutting, and then they were ground and polished to remove the oxide layer that may be formed during cutting. Figs. 10 and 11 show the SEM morphologies of the cross-sections for case 6 and case 7, respectively. It is clearly seen that there is an affecting layer after laser irradiation in nitrogen atmosphere, which shows very different microstructures with the MG matrix. Furthermore, EDS line tests were performed along the depth direction of the cross-sections. The line 1 and line 2 stand for the measuring origination for case 6 and case 7, respectively. The corresponding results are illustrated in Figs. 12 and 13, respectively. From Figs. 12 and 13, it can be qualitatively seen that the concentrations of Zr and N elements in the affecting layer are higher than those in the MG matrix, which well demonstrates the existence of the affecting layer after mechanical polishing. From Figs. 10–13, it is obtained that for case 6, the depth of the affecting layer after laser irradiation is about 92 μm, and it is reduced to about 80 μm after mechanical polishing; while for case 7, it is about 44 μm after laser irradiation and it is reduced to about 40 μm after mechanical polishing. By comparing the laser parameters in Table 5, the larger depth of the affecting layer for case 6 is mainly due to the higher laser power, which results in a larger molten pool and thus larger depth of the affecting

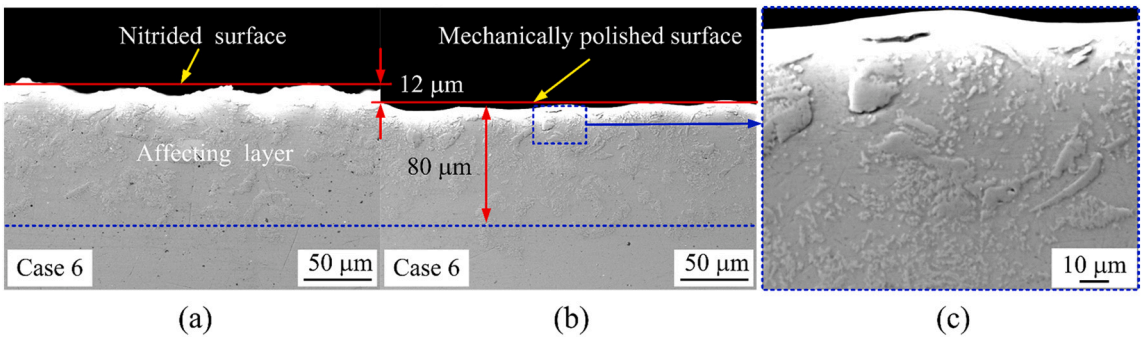

Fig. 10. (a) and (b) show the SEM morphologies of the cross-sections before and after mechanical polishing for case 6. (c) Local enlarged view of panel (b).

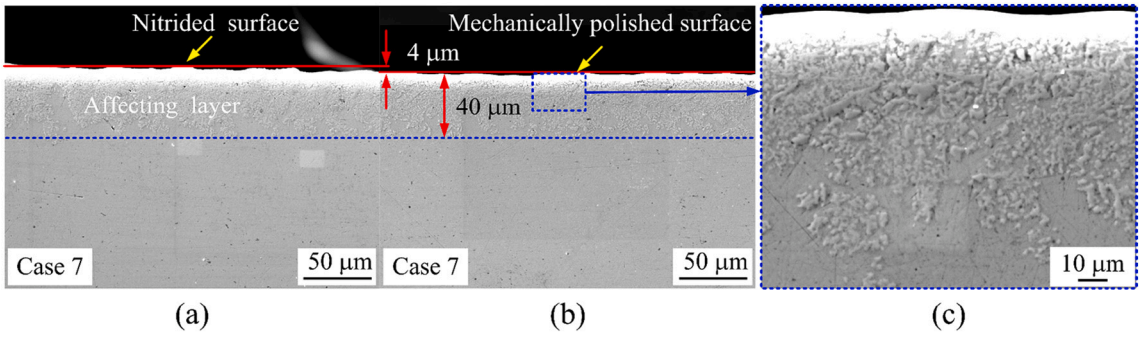

Fig. 11. (a) and (b) show the SEM morphologies of the cross-sections before and after mechanical polishing for case 7. (c) Local enlarged view of panel (b).

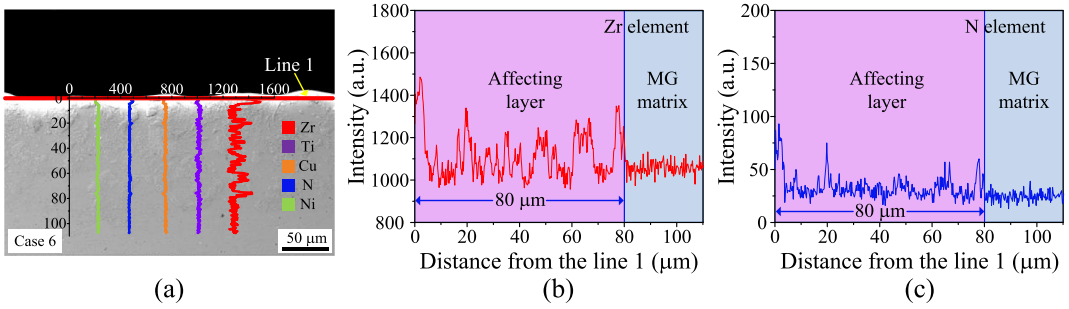

Fig. 12. EDS line test performed on the cross-section for case 6. (a) Indicates the cross-sectional region where the EDS test is performed; (b) and (c) illustrate the distribution of Zr and N elements along the depth direction of the cross-section, respectively.

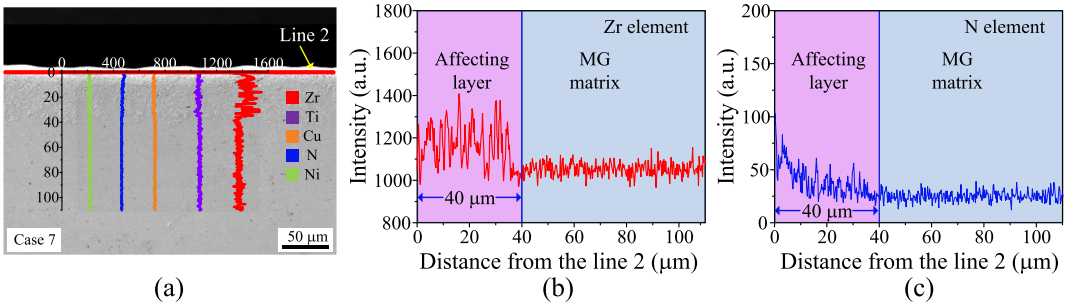

Fig. 13. EDS line test performed on the cross-section for case 7. (a) Indicates the cross-sectional region where the EDS test is performed; (b) and (c) illustrate the distribution of Zr and N elements along the depth direction of the cross-section, respectively.

layer. In Figs. 10(c) and 11(c), it is noted that the affecting layer is covered by a large number of cluster structures, which could be the nitride phases by analyzing the XRD patterns in Fig. 7. Furthermore, the cluster structures for case 7 are much finer and uniform compared to those for case 6, and this could be due to the higher overlap rate and the increased number of irradiation cycle for case 7. From Table 6, Figs. 7, 10–13, it can be concluded that the surface hardness of the irradiated surface is related to the content of ZrN phase as well as its morphology and distribution, which could be further tuned by the employed laser parameters.

4. Conclusions

In summary, a $L_{64}(4 \times 8^3)$ orthogonal array was designed to explore the potential of laser nitriding for improving the surface hardness of Zr-based MG. By systematic experiments and analysis, the following conclusions could be obtained.

(1) Under some given laser parameters, surface hardness of Zr-based MG has been significantly increased by laser irradiation in nitrogen atmosphere, and the increase in surface hardness is attributed to the generation of ZrN phase.
(2) For the employed laser parameters, the average laser power and scanning speed have a stronger influence on the surface hardness compared to the overlap rate and number of irradiation cycle.
(3) Laser irradiation in nitrogen atmosphere affects the micro-scale plastic deformation of Zr-based MG, and the surface shear bands around the indentation and serrated flows in the load-depth curve present significant difference compared to the as-case MG surface.
(4) An affecting layer consisting of nitride phase have been formed after laser irradiation in nitrogen atmosphere, and its depth is affected by the employed laser parameters.

This study confirms that nanosecond pulsed laser irradiation in nitrogen atmosphere is a feasible method to greatly improve the surface hardness of Zr-based MG, which could enhance its functional applications as surface contact materials. In our future study, the interfacial characteristics between the nitride phase and the MG matrix would be further investigated by the transmission electron microscopy (TEM).

CRediT authorship contribution statement

Jing Hong: Investigation, Formal analysis, Data curation, Writing – original draft. **Yongfeng Qian:** Investigation, Writing – original draft. **Lin Zhang:** Investigation, Data curation. **Hu Huang:** Conceptualization, Funding acquisition, Methodology, Investigation, Resources, Supervision, Writing – review & editing. **Minqiang Jiang:** Investigation, Methodology. **Jiwang Yan:** Supervision.

Declaration of competing interest

The authors declare that they have no known competing financial interests or personal relationships that could have appeared to influence the work reported in this paper.

Acknowledgements

This work was supported by the National Natural Science Foundation of China (Grant No. 51705197), the Graduate Innovation Fund of Jilin University (Grant No. 101832020CX106), and the Fundamental Res earch Funds for the Central Universities (2019–2021).

References

[1] W.H. Wang, C. Dong, C.H. Shek, Bulk metallic glasses, Mater. Sci. Eng. R 44 (2008) 45–89.
[2] B.J. Schroers, Processing of bulk metallic glass, Adv. Mater. 22 (2010) 1566–1597.
[3] M.M. Khan, A. Nemati, Z.U. Rahman, U.H. Shah, H. Asgar, W. Haider, Recent advancements in bulk metallic glasses and their applications: a review, Crit. Rev. Solid State 43 (2018) 233–268.
[4] M.M. Trexler, N.N. Thadhani, Mechanical properties of bulk metallic glasses, Prog. Mater. Sci. 55 (2010) 759–839.
[5] W.B. Wang, H. Mraied, W. Diyatmika, J.P. Chu, W.J. Cai, Effects of nanoscale chemical heterogeneity on the wear, corrosion, and tribocorrosion resistance of Zr-based thin film metallic glasses, Surf. Coat. Technol. 402 (2020), 126324.
[6] J. Schroers, Bulk metallic glasses, Phys. Today 66 (2013) 32–37.
[7] J.W. Qiao, H.L. Jia, P.K. Liaw, Metallic glass matrix composites, Mater. Sci. Eng. R 100 (2016) 1–69.
[8] B. Gludovatz, D. Granata, K.V.S. Thurston, J.F. Loffler, R.O. Ritchie, On the understanding of the effects of sample size on the variability in fracture toughness of bulk metallic glasses, Acta Mater. 126 (2017) 494–506.
[9] Z. Wang, J.W. Qiao, G. Wang, K.A. Dahmen, P.K. Liaw, Z.H. Wang, B.C. Wang, B. S. Xu, The mechanism of power-law scaling behavior by controlling shear bands in bulk metallic glass, Mater. Sci. Eng. A 639 (2015) 663–670.
[10] M.Q. Jiang, L.H. Dai, Shear-band toughness of bulk metallic glasses, Acta Mater. 59 (2011) 4525–4537.
[11] C.W. Chan, S. Lee, G.C. Smith, C. Donaghy, Fibre laser nitriding of titanium and its alloy in open atmosphere for orthopaedic implant applications: investigations on surface quality, microstructure and tribological properties, Surf. Coat. Technol. 309 (2017) 628–640.
[12] C.L. Donaghy, R. McFadden, S. Kelaini, L. Carson, A. Margariti, C.W. Chan, Creating an antibacterial surface on beta TNZT alloys for hip implant applications by laser nitriding, Opt. Laser Technol. 121 (2020), 105793.
[13] N. Ohtsu, W. Saito, M. Yamane, Parameter settings in a compact laser-nitriding system for titanium composed of a focused pulsed Nd:YAG laser and nitrogen gas blow, Surf. Interface. Anal. 51 (2019) 302–307.
[14] C.H. Ng, C.W. Chan, H.C. Man, D.G. Waugh, J. Lawrence, NiTi shape memory alloy with enhanced wear performance by laser selective area nitriding for orthopaedic applications, Surf. Coat. Technol. 309 (2017) 1015–1022.
[15] A.R. Kulkarni, M. Manikandan, A.K. Shukla, S. Subramaniam, V.P. Balaji, I. A. Palani, M. Jayaprakash, Influence of laser-nitriding on mechanical and elevated temperature fretting wear behavior of A356-alloy, Surf. Coat. Technol. 413 (2021), 127072.
[16] H. Huang, M.Q. Jiang, J.W. Yan, The coupling effects of laser thermal shock and surface nitridation on mechanical properties of Zr-based metallic glass, J. Alloy Compd. 770 (2019) 864–874.
[17] H.N. Meng, Z.Z. Zhang, F.X. Zhao, T. Qiu, J.D. Yang, Orthogonal optimization design for preparation of Fe_3O_4 nanoparticles via chemical coprecipitation, Appl. Surf. Sci. 280 (2013) 679–685.
[18] J. Zhou, C.H. Liao, H. Shen, X.H. Ding, Surface and property characterization of laser polished Ti6Al4V, Surf. Coat. Technol. 380 (2019), 125016.
[19] B. Jiang, M. Wu, M. Zhang, F. Zhao, Z.G. Zhao, Y.Z. Liu, Microstructural characterization, strengthening and toughening mechanisms of a quenched and tempered steel: effect of heat treatment parameters, Mater. Sci. Eng. A 707 (2017) 306–314.
[20] W. Oliver, G. Pharr, An improved technique for determining hardness and elastic modulus using load and displacement sensing indentation experiments, J. Mater. Res. 7 (1992) 1564–1583.
[21] Y.S. Li, K. Zhang, Y. Wang, W.Q. Tang, Y.T. Zang, B.C. Wei, Z. Hu, Abnormal softening of Ti-metallic glasses during nanosecond laser shock peening, Mater. Sci. Eng. A 773 (2020), 138844.
[22] Y.H. Gu, H. Kodama, E. Ogawa, Y. Izumi, Lactate and pyruvate levels in blood and cerebrospinal fluid in patients with menkes disease, J. Pediatr. 164 (2014) 890–894.
[23] Y.H. Zhu, J. Fu, C. Zheng, Z. Ji, Structural and mechanical modifications induced on Zr-based bulk metallic glass by laser shock peening, Opt. Laser Technol. 86 (2016) 54–60.
[24] J.L. Cheng, G. Chen, W. Zhao, Z.Z. Wang, Z.W. Zhang, Enhancement of tensile properties by the solid solution strengthening of nitrogen in Zr-based metallic glass composites, Mater. Sci. Eng. A 696 (2017) 461–465.
[25] A. Bolshakov, G.M. Pharr, Influences of pileup on the measurement of mechanical properties by load and depth sensing indentation techniques, J. Mater. Res. 13 (1998) 1049–1058.
[26] D. Prof Gunnar, Meyer's hardness law and its relation to other measures of ball hardness tests, Cryst. Res. Technol. 32 (1997) 149–154.
[27] L. Wang, L. Wang, Z.H. Nie, Y. Ren, Y.F. Xue, R.H. Zhu, H.F. Zhang, H.M. Fu, Evolution of residual stress, free volume, and hardness in the laser shock peened Ti-based metallic glass, Mater. Des. 111 (2016) 473–481.
[28] X. Liu, J. Kong, X.X. Song, S. Feng, Z.B. Zhang, Y. Yang, T.C. Wang, Free volume evolution dominated by glass forming ability determining mechanical performance in $Zr_xTi_{65-x}Be_{27.5}Cu_{7.5}$ metallic glasses, Mater. Sci. Eng. A 804 (2021), 140764.
[29] N.C. Reger, V.K. Balla, M. Da, A.K. Bhargava, Wear and corrosion properties of in-situ grown zirconium nitride layers for implant applications, Surf. Coat. Technol. 334 (2017) 357–364.
[30] H. Huang, J.W. Yan, Investigating shear band interaction in metallic glasses by adjacent nanoindentation, Mater. Sci. Eng. A 704 (2017) 375–385.
[31] F.C. Li, M. Song, S. Ni, S.F. Guo, X.Z. Liao, Correlation between hardness and shear banding of metallic glasses under nanoindentation, Mater. Sci. Eng. A 657 (2016) 38–42.
[32] S.H. Chen, H. Tang, H.M. Zheng, W.J. Chang, R.P. Liu, Achieving stable plastic flows in a Zr-based bulk metallic glass under tailored mixed-mode (I/II) loading conditions, Mater. Sci. Eng. A 772 (2019), 138695.
[33] M.C. Li, M.Q. Jiang, F. Jiang, L. He, J. Sun, Testing effects on hardness of a Zr-based metallic glass under nanoindentation, Scripta Mater. 138 (2017) 120–123.
[34] J.L. Wu, Y. Pan, J.H. Pi, Evaluation of Cu-Zr-Ti-In bulk metallic glasses via nanoindentation, J. Mater. Eng. Perfom. 22 (2013) 2288–2292.
[35] J. Fu, Y.H. Zhu, C. Zheng, R. Liu, Z. Ji, Effect of laser shock peening on the compressive deformation and plastic behavior of Zr-based bulk metallic glass, Opt. Laser Technol. 86 (2016) 53–61.
[36] X.M. Cui, Z.L. Yu, F. Liu, Z.X. Du, P.C. Bai, Influence of secondary phases on crack initiation and propagation during fracture process of as-cast Mg-Al-Zn-Nd alloy, Mater. Sci. Eng. A 759 (2019) 708–714.